JOURNAL OF SPACECRAFT AND ROCKETS
Vol. 44, No. 6, November–December 2007

Polymer Nanostructured Materials for Propulsion Systems

Joseph H. Koo*
University of Texas at Austin, Austin, Texas 78712-0292
and
Louis A. Pilato† and Gerry E. Wissler‡
KAI, LLC, Austin, Texas 78739-1510

DOI: 10.2514/1.26295

The introduction of inorganic nanomaterials as additives into polymer systems has resulted in polymer nanostructured materials exhibiting a multiplicity of high-performance characteristics beyond what traditional polymer composites possess. These multifunctional features attributable to polymer nanocomposites consist of improved thermal and flame resistance, moisture and chemical resistance, decreased permeability, charge dissipation, and thermal/electricity conductivity. Through control/alteration of the additive at the nanoscale level, one is able to maximize property enhancement of selected polymer systems to meet or exceed the requirements of current commercial, military, and aerospace applications. The technical approach involves the introduction of nanoparticles into selected polymer matrix systems whereby nanoparticles may be surface-treated to provide hydrophobic characteristics and enhanced inclusion into the hydrophobic polymer matrix. The objectives of this paper are to summarize our current research efforts in the use of polymer nanostructured materials for high-temperature applications such as rocket nozzle ablative materials, resulting in lower ablation rates and reduced backside temperatures, carbon–carbon composites with improved thermo-oxidative resistance, and enhanced damage-tolerant high-performance epoxy matrix resin, but not carried over to carbon-fiber-reinforced composite systems.

I. Introduction

THE introduction of inorganic nanomaterials as additives into polymer matrix systems has resulted in polymer nanocomposites exhibiting multifunctional high-performance polymer characteristics beyond what traditional polymer composites possess. Multifunctional features attributable to polymer nanocomposites consist of improved thermal and flame resistance, chemical resistance, moisture resistance, decreased permeability, charge dissipation, and thermal/electrical conductivity. Through control/adjustment of the additive at the nanoscale level, one is able to maximize property enhancement of selected polymer systems to meet or exceed the requirements of current military, aerospace, and commercial applications. Selected polymer nanocomposites are being examined as high-temperature materials for solid rocket combustion gases/exhaust plume protection, thermo-oxidative-resistant, and high-performance polymer matrix composites (PMCs). Selective thermosets, thermoplastics, and elastomers have been used with montmorillonite (MMT) organoclays, nanosilicas, carbon nanofibers (CNFs), polyhedral oligomeric silsesquioxane (POSS®), and carbon nanotubes to solve specific government and industry problems [1].

The technical approach involves the introduction of nanoparticles into selected polymer matrix systems. The nanoparticles may be surface-treated to provide hydrophobic characteristics and enhanced inclusion into the hydrophobic polymer matrix (e.g., nanoclays, coreact/cocure with polymer matrix such as POSS, or intimately mixed CNF with polymer matrix, and others). Several high-shear processing techniques to uniformly disperse the nanoparticles are identified. Polymer nanocomposites (PNCs) are characterized by wide-angle x-ray diffraction (WAXD), transmission electron microscopy (TEM), and scanning electron microscopy (SEM) to determine whether nanoparticles are distributed uniformly within the polymer matrix. Further processing–structure–property relationships of these novel polymer nanocomposites are discussed, as well as the performance of these materials for high-temperature applications involving simulated solid rocket motor or other test methods.

The following research topics will illustrate the technical approach: 1) nanocomposite rocket ablative materials (NRAMs) for solid rocket nozzles; 2) nanomodified carbon–carbon composites (NCCCs) for thermo-oxidative-resistant structures; and 3) nanocomposites for carbon-fiber-reinforced polymer matrix composites (NCPMCs) for missile/airframe structures

II. Selection of Materials

A. Polymer Systems

Different types of polymers such as thermosets, thermoplastics, and thermoplastic elastomers can be nanomodified [1]. Selected examples with different polymer types are discussed and include thermosetting resins such as phenolic, cyanate ester, and epoxy.

B. Polymer Nanoparticles

Four types of nanoparticles were used in this study: namely, Southern Clay Products' MMT nanoclays, Applied Sciences' CNFs, Degussa's nanosilica materials, and Hybrid Plastics' POSS [1]. These nanoparticles will reinforce the polymer in the nanoscale and will enhance the dimensional stability and mechanical properties of the polymer nanocomposites. To achieve the potential improvements, nanoparticles usually require some degree of dispersion and exfoliation (for MMT nanoclays). These are shown to be dependent upon a combination of proper chemical treatment and optimized processing.

Presented as Paper 3606 at the 41st AIAA/ASME/SAE/ASEE Joint Propulsion Conference, Tucson, AZ, 10–13 July 2005; received 2 July 2006; revision received 17 June 2007; accepted for publication 17 June 2007. Copyright © 2007 by the American Institute of Aeronautics and Astronautics, Inc. All rights reserved. Copies of this paper may be made for personal or internal use, on condition that the copier pay the $10.00 per-copy fee to the Copyright Clearance Center, Inc., 222 Rosewood Drive, Danvers, MA 01923; include the code 0022-4650/07 $10.00 in correspondence with the CCC.

*Senior Research Scientist/Director, Solid Freeform Fabrication Consortium, Mechanical Engineering Deptartment, 1 University Station, C2200; jkoo@mail.utexas.edu. Associate Fellow AIAA (Corresponding Author).
†Chief Scientist.
‡Senior Scientist, 6402 Needham Lane.

1. Montmorillonite Nanoclays

Nanoclay is the most widely investigated nanoparticle in a variety of different polymer matrices for a spectrum of applications [1–3]. Exfoliation of these nanoclays into a polymer has been shown to increase mechanical properties, barrier performance, and application processing. To achieve exfoliation requires surface treatment of the MMT clays and high-shear mixing efficiency of the dispersing apparatus. Exchanging MMT clay inorganic counterions, sodium, with long chain quaternary ammonium ions results in surface treatment of MMT clay with satisfactory hydrophobic characteristics and ease of dispersing the surface-treated nanoclays within the hydrophobic polymer continuous phase. Selective nanoclays from Southern Clay Products were examined in our studies [1].[§]

2. Nanosilica

Aerosil® nanosilica is highly dispersed, amorphous, very pure silica that is produced by high-temperature hydrolysis of silicon tetrachloride in an oxyhydrogen gas flame [1]. The primary particles are spherical and free of pores. The average diameters of the primary particles are about 7 to 40 nm. Siloxane and silanol groups are situated on the surface and are responsible for the hydrophilic behavior of untreated Aerosil. Different grades of hydrophilic and hydrophobic Aerosil nanosilicas are available from Degussa [1].[¶]

3. Carbon Nanofibers

CNFs are a form of vapor-grown carbon fiber (VGCF), which is a discontinuous graphitic filament produced in the gas phase from the pyrolysis of hydrocarbons [1,4–6]. CNFs are intermediate between carbon black (CB), fullerenes, and single-wall to multiwall carbon nanotubes on one end and continuous carbon fiber on the other. CNFs are able to combine many advantages of these other forms of carbon for reinforcement in commodity and high-performance engineering polymers. An excellent review of carbon nanotubes and nanofibers in composite materials was published by Maruyama and Alam [7], and a recent review of the fabrication and properties of VGCF in polymer composites was published by Tibbetts et al. [6]. CNFs are available in diameters ranging from 50 to 200 nm and lengths of 50 to 100 μm. CNFs are manufactured by Applied Sciences, Inc./Pyrograf Products [1].[**]

4. Polyhedral Oligomeric Silsesquioxane

POSS nanostructured materials, representing a merger between chemical and filler technologies, can be used as multifunctional polymer additives, acting simultaneously as molecular level reinforcements, processing aids, and flame retardants. POSS possesses two unique structural features:

1) The chemical composition is a hybrid, intermediate ($RSiO_{1.5}$) between that of silica (SiO_2) and silicones (R_2SiO).

2) POSS molecules are nanoscopic in size, ranging from approximately 1 to 3 nm. These materials have multifunctional properties and an inorganic framework of silicone oxide, ceramiclike in nature, especially in severe environments. POSS nanostructured materials are available from Hybrid Plastics [1].[††]

III. Processing and Characterization of Nanoparticles in Polymer Systems

A. Processing of Nanoparticles into Polymers

In general, for solid thermosetting reactive prepolymer or thermoplastic polymers with solid nanoparticles, the following processing methods are recommended [1]: Solution intercalation, melt intercalation, and roll mixing. The solution intercalation method requires that the desired polymer is soluble in a solvent, and the appropriate nanoparticle is intercalated/exfoliated into the single layers or in small aggregates within the polymer solution. The method of melt intercalation consists of mixing solid polymer matrix and nanoparticle in the molten state. If the layer surfaces of the nanoparticle are sufficiently compatible with the selected particle, the polymer can be inserted into the interlayer space and form an intercalated or exfoliated nanocomposite for which no solvent is required. Roll mixing is a technique for low-shear mixing for introducing solid nanoparticles into a liquid polymer and differs from high-shear mixing (discussed later). It is reasonably cost-effective and results in optimum dispersion uniformity.

For liquid thermosetting reactive prepolymer with solid nanoparticles, the following processing methods are recommended [1]: in situ polymerization, emulsion polymerization, and high-shear mixing. The in situ or emulsion polymerization methods require the polymerization of monomer(s) with layered nanoclay dispersed in an aqueous phase (emulsion method) or involves the layered nanoclay swollen within the liquid monomer or monomer solution so that polymer formation can occur between intercalated sheets. High-shear mixing is achieved when nanoparticles are mixed with liquid reactive thermosetting oligomers using high-shear equipment (IKA® mixer, IKA Works). If the surface-treated nanoparticles are compatible with the selected oligomer, the high-shear mixing will disrupt the nanoparticle aggregates and disperse the oligomer into the nanocomposite layers. Both liquid and semisolid oligomers were used in this study.

B. Characterization of Polymer Nanostructured Materials

Dispersibility of nanoparticles in different polymers to characterize the level and uniformity of nanoparticle dispersion (nanoclay) within the polymer continuous phase is monitored by using WAXD, which measures the spacing between the ordered crystalline layers of organoclay (see Fig. 1). TEM is critical instrumentation due to the extremely small particle size of the added nanoparticles. TEM provides a real space image on the atom distribution in the nanocrystal and its surface within the resulting nanocomposite continuous phase. It allows observation of the overall characteristics of uniformity or nonuniformity of nanoparticles dispersed in the polymer matrix. SEM is used to observe morphology and resulting pyrolyses of ablative composites, especially NRAMs after posttest conditions.

Structure–property relationships such as glass transition temperature T_g and complex modulus E^* of polymer, especially for nanomodified epoxy resins (NCPMCs), are characterized using dynamic mechanical thermal analyses (DMTAs).

Thermal performance of the resulting nanostructured materials for different applications are evaluated using established laboratory devices such as simulated solid rocket motor (SSRM) and subscale solid rocket motor. The SSRM is a small-scale liquid-fueled rocket motor burning a mixture of kerosene and oxygen as shown in Fig. 2. Aluminum oxide particles are injected into the plume to simulate the particle-laden flow of solid rocket exhaust plumes. It is capable of developing heat fluxes of 40 to 1250 $\mathrm{Btu/ft^2 \cdot s}$ (454 to $14,200\ \mathrm{kW/m^2}$), flame temperature of 3992°F (2200°C), and velocity of the particle-laden exhaust of approximately 2000 m/s. The sample size is 4 by 4 by $\frac{1}{4}$ or $\frac{1}{2}$ in. thick (10.2 by 10.2 by 0.64 or 1.28 cm thick). This device was used to evaluate materials performance for rocket propulsion applications.

Mechanical properties of NCCCs and NCPMCs were determined by American Society for Testing and Materials (ASTM) standards such as tensile strength and modulus; Poisson's ratio per ASTM D-3039-00 (minimum of three specimens); interlaminar shear (ILSS) using a four-point short-beam shear test per ASTM D-7904 (minimum of three specimens); interlaminar fracture toughness, G_{1C}, and G_{2C} per ASMT E-399 (minimum of five specimens); flatwise tension strength (FWT) per ASTM C-297 (minimum of five specimens); short-beam interlaminar shear strength (SBS) per

[§]Technical data sheet available online at http://www.nanoclay.com [retrieved 6 April 2007].

[¶]Technical data sheet available online at http://www.aerosil.com [retrieved 6 April 2007].

[**]Technical data sheet available online at http://www.apsci.com [retrieved 6 April 2007].

[††]Technical data sheet available online at http://www.hybridplastics.com [retrieved 6 April 2007].

ASTM D-7904 (minimum of five specimens); and flexural strength per ASTM D-790 (minimum of five specimens).

IV. Discussion of Results

The challenges to form PNCs involve the choice of nanoparticles, proper processing techniques, and selective analytical characterization of nanocomposite morphology. Several application areas using nanocomposite methodology will be discussed in this paper, such as nanocomposite rocket ablative materials, nanomodified carbon–carbon composites, and nanocomposites for carbon-fiber-reinforced polymer matrix composites. The starting materials for these studies are reactive thermosetting oligomers, which are semisolid or liquid. Our studies were guided by the introduction of low amounts of nanoparticles (less than or equal to 10 wt %) to minimize high viscosity of the resulting nanomodified oligomer, except when larger amounts of CNF (up to 28 wt %) were used in NRAMs. Besides substantial viscosity increase, higher amounts of nanoparticles greater than 10 wt % in nanocomposite resulted in a reduction of properties.

A. Nanocomposite Rocket Ablative Materials

This study is aimed at developing NRAMs for solid rocket nozzles [1,8–12]. Both WAXD and TEM methods are used to determine dispersion uniformity before full ablation testing, which is expensive. Borden SC-1008 resole phenolic resin in isopropanol alcohol is the baseline resin system. The commercial material, MX-4926, is a rayon carbon fabric impregnated with SC-1008 containing CB particles. When dispersing nanoclay into the resole phenolic resin with CB, followed by cure and examination by WAXD and TEM, it was concluded that CB particles in the baseline MX-4926 caused interference during dispersion of the nanoparticles in the resole phenolic resin. As a result, CB was eliminated in subsequent blending experiments. Use of nanoclay, Cloisite® 30B from Southern Clay Products, in loadings of 5, 10, and 15 wt % indicated that the nanoparticles dispersed satisfactorily into the SC-1008. Figure 1 shows the WAXD of the three nanoclay loadings in SC-1008 and indicates good dispersibility of the nanoclay into SC-1008. TEM images of nanoclay with SC-1008 are shown in Figs. 3–5. The TEM images indicate intercalation and not exfoliation of the nanoclay in the resin system. The TEM analyses were very convenient in determining the degree of dispersion/exfoliation and were a cost-effective and efficient technique for screening different formulations before committing to a large quantity of material.

The SC-1008 with 5, 10, and 15 wt % Cloisite 30B replaced the 15 wt % CB in the original MX-4926 formulation. Table 1 illustrates the different loadings of Cloisite 30B [$(HE)_2MT$] and trisilanolphenyl-POSS (SO-1458) in the rayon-fabric-reinforced SC-1008 system. When a small amount of CNF (less than 1.5 wt %) was added in the SC-1008 phenolic resin, the viscosity of the resin

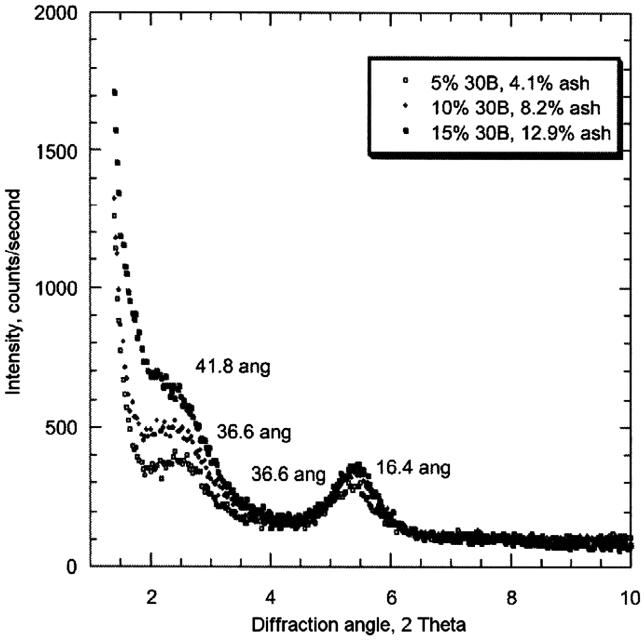

Fig. 1 WAXD data showing the intensity of 5, 10, and 15% of Cloisite 30B MMT nanoclay in resole phenolic.

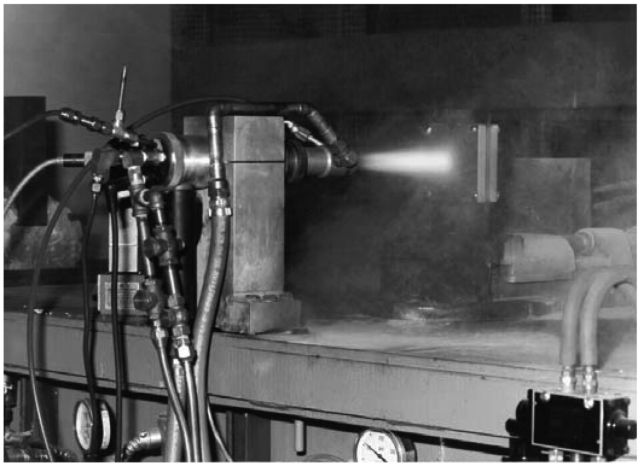

Fig. 2 SSRM testing ablative candidates.

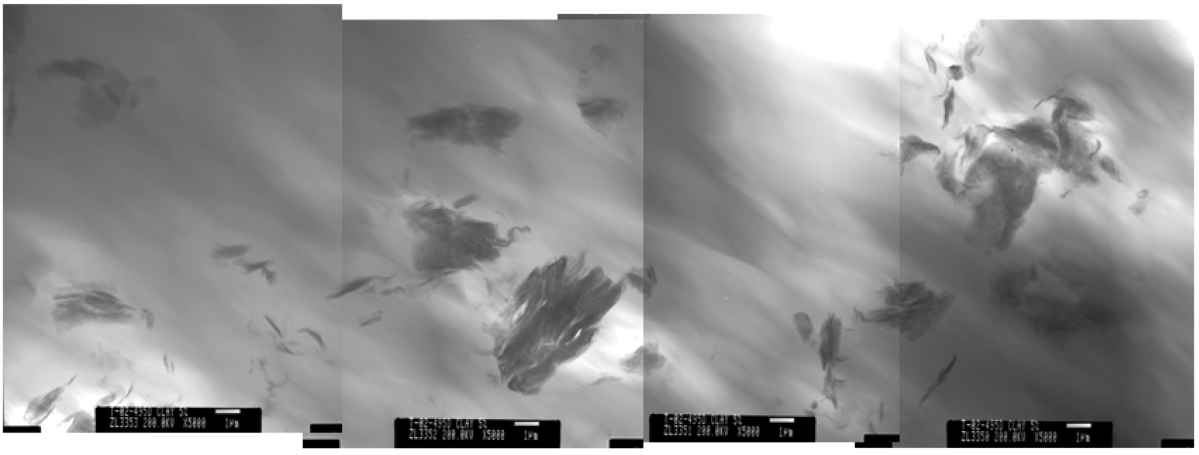

Fig. 3 TEM images of 5 wt % Cloisite 30B in 95 wt % SC-1008 (scale bar is 1 μm).

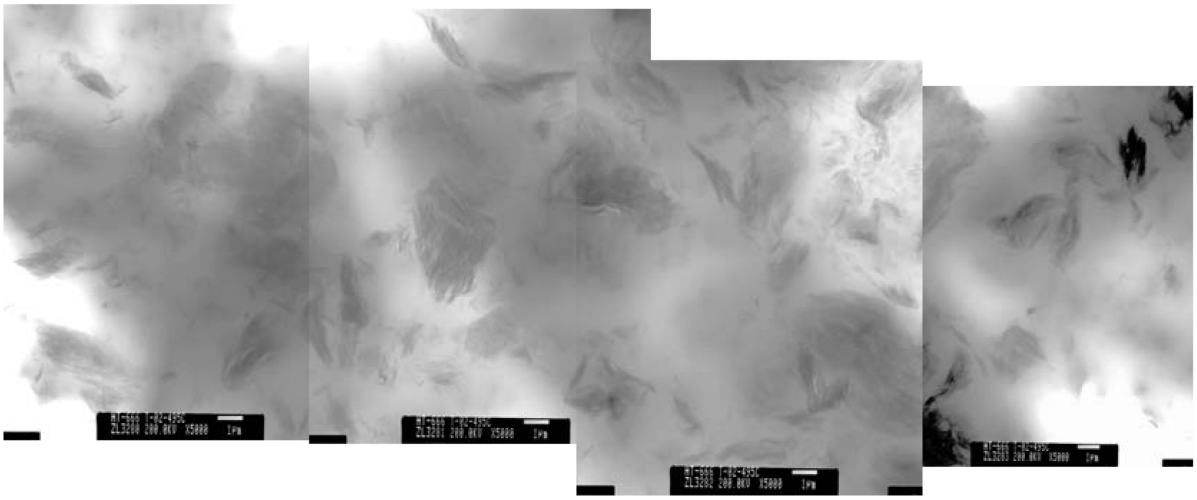

Fig. 4 TEM images of 10 wt % Cloisite 30B in 90 wt % SC-1008 (scale bar is 1 μm).

increased significantly. It was impossible to process carbon prepregs under these conditions. It was decided that a molding compound will be fabricated to include large loadings of CNF dispersed in the SC-1008 resin. As a result, three loadings of PR-24-PS CNF at 20, 24, and 28 wt % were dispersed into SC-1008 without the rayon fabric reinforcement. Compositions and densities of the NRAMs are shown in the Table 1. These nanomodified composites were manufactured and fabricated by Cytec Engineered Materials. A plot of density vs nanoparticle loading is illustrated in Fig. 6 and shows that the nanomodified materials are lower in density than the baseline material, MX-4926.

The SSRM is a small-scale supersonic liquid-fueled rocket motor burning a combination of kerosene and oxygen. It was used to study the ablation and insulative characteristics of the ablatives (Fig. 2). The SSRM has been demonstrated to be a very cost-effective laboratory device to evaluate ablatives under identical conditions for initial screening and development [13,14]. Peak erosion of MX-4926 and the three nanoclay {Cloisite 30B [$(HE)_2MT$]} compositions at three heat fluxes with Al_2O_3 particles is shown in Fig. 7. As expected, peak erosion decreases as heat flux is decreased. At high heat flux (1.2×10^4 kW/m^2) the baseline and nanoclay compositions exhibit a noticeable spread in erosion depth, whereas the medium and low heat flux conditions show little difference in peak erosion. Compositions with 2.5 and 5 wt % $(HE)_2MT$ are not as erosion-resistant as the control, MX-4926. The 7.5% composition exhibited better erosion characteristics than MX-4926 by 14%. A comparison of maximum backside heat-soaked temperature rise indicates that all the nanoclay compositions were lower than MX-4926 by 28% (Fig. 8). Surface temperatures of the nanoclays are also lower than MX-4926 (Fig. 9).

Data for PR-19-PS and PR-24-PS CNF/SC-1008 systems (without rayon fabric) demonstrate that the CNF NRAM systems exhibit better ablation resistance than the control, MX-4926 at high heat flux level by about 42% lower (Fig. 10). Maximum backside heat-soaked temperature rise values are substantially lower than MX-4926 by about 68% at all three levels of heat fluxes (Fig. 11). The surface temperature of the CNF NRAMs was hotter than that of MX-4926, the clay NRAMs, and the POSS NRAMs (Fig. 12). This suggests that better radial heat transfer than axial heat transfer is occurring with the CNF NRAMs and is supported by the glowing heat of the surface observed during materials testing.

The ablation rates (Fig. 13) of MX-4926 and all three nanoparticles indicate that only 7.5% nanoclay composition shows a lower ablation rate than MX-4926, which is about 0.4 mm/s. All three CNF compositions are lower than MX-4926, with the 28% CNF NRAM being the lowest. All three POSS compositions have lower ablation rate, with the 5% POSS NRAM being the lowest. The residual mass (Fig. 14) of MX-4926 is about 92%. The POSS NRAMs exhibited the highest of all the nanoparticles in residual mass, or about 93%. The clay NRAMs were comparable to MX-4926, whereas the CNF NRAMs were lower. A summary of backside temperature rise is shown in Fig. 15, with all the nanoparticles compositions exhibiting lower maximum backside heat-soaked temperature rise than MX-4926. The value of MX-4926 is 106°C, with CNF NRAMs being the lowest, from 54 to 72°C. The POSS NRAMs were intermediate, from 75 to 86°C, with clay NRAMs being the highest of the nanoparticles, from 82 to 98°C, but still below the MX-4926 value of 106°C.

An infrared pyrometer was used to measure the surface temperatures of all materials during SSRM firings. Figure 16 shows

Table 1 Specimen configuration for SSRM laminates fabrication

Material ID	Density, g/cm^3	Rayon carbon fiber reinforcement, wt %	Resin SC-1008 phenolic, wt %	Filler, wt %
MX-4926 (control)	1.44	50	35	15 carbon black (CB)
MX-4926 ALT clay 5%	1.42	50	47.5	2.5 Cloisite 30B [$(HE)_2MT$]
MX-4926 ALT clay 10%	1.43	50	45	5 Cloisite 30B [$(HE)_2MT$]
MX-4926 ALT clay 15%	1.43	50	42.5	7.5 Cloisite 30B [$(HE)_2MT$]
PR-24-PS 20%/SC-1008	1.35	None	80	20 PR-24-PS CNF
PR-24-PS 24%/SC-1008	1.38	None	76	24 PR-24-PS CNF
PR-24-PS 28%/SC-1008	1.41	None	72	28 PR-24-PS CNF
MX4926 ALT SO-1458 2%	1.41	50	49	1 Trisilanolphenyl-POSS [SO-1458]
MX4926 ALT SO-1458 6%	1.38	50	47	3 Trisilanolphenyl-POSS [SO-1458]
MX4926 ALT SO-1458 10%	1.40	50	45	5 Trisilanolphenyl-POSS [SO-1458]

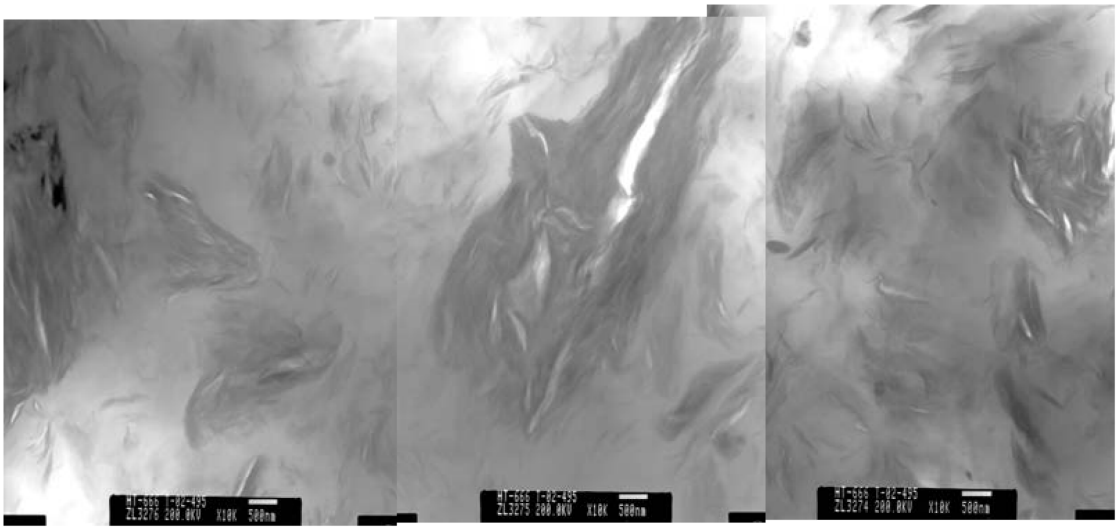

Fig. 5 TEM images of 15 wt % Cloisite 30B in 85 wt % SC-1008 (scale bar is 500 nm).

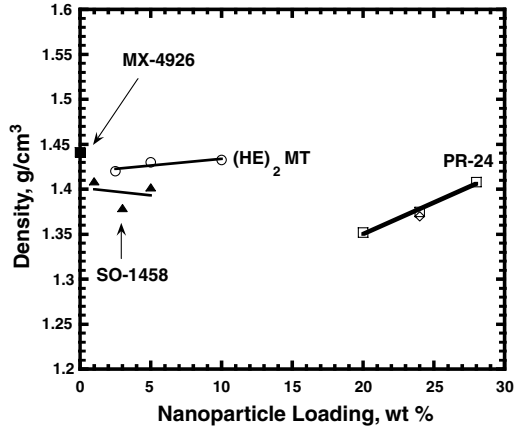

Fig. 6 Density of MX-4926 and NRAMs with different nanoparticle loadings.

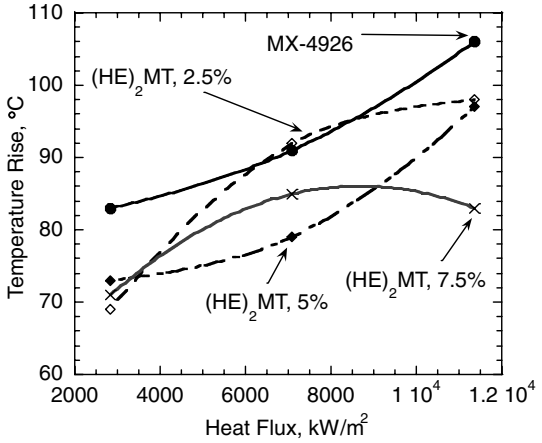

Fig. 8 Maximum backside heat-soaked temperature rise for MX-4926 and three loadings of clay NRAMs at three different heat flux levels with particles.

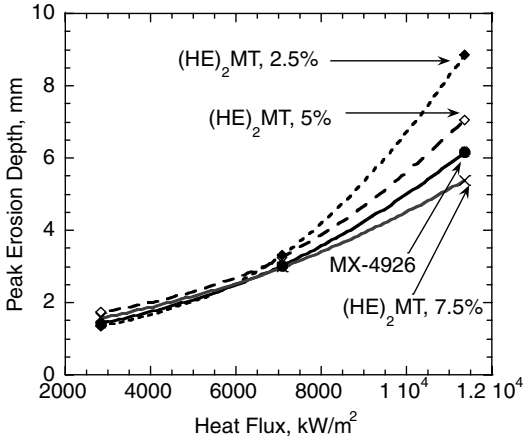

Fig. 7 Peak erosion for MX-4926 and three loadings of clay NRAMs at three different heat flux levels with particles.

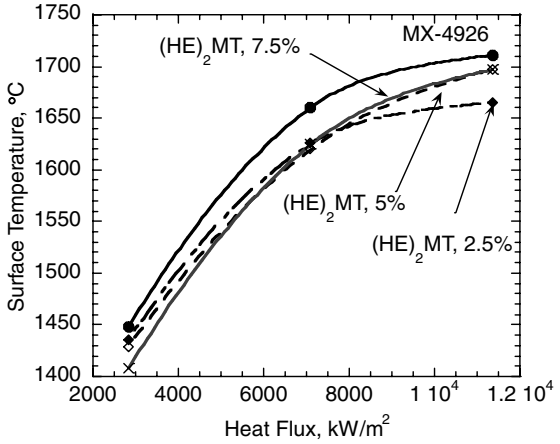

Fig. 9 Surface temperature for MX-4926 and three loadings of clay NRAMs at three different heat flux levels with particles.

the surface temperatures of MX-4926 (1700°C) and the NRAMs. Surface temperatures of the CNF NRAMs samples were higher than those of MX-4926, the clay NRAMs, and the POSS NRAMs. This finding suggests that better radial heat transfer is occurring rather than axial heat transfer. This is supported by the glowing heat of the material surface observed during material testing. This phenomenon was observed by other researchers [15] and needs further study. The surface temperatures of clay NRAMs and POSS NRAMs were lower than those of MX-4926. The amount of nanoclay in the clay NRAMs

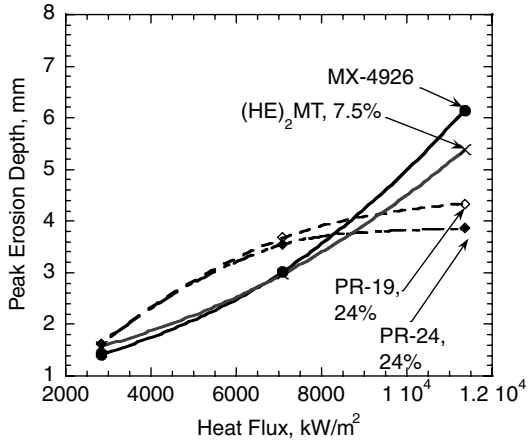

Fig. 10 Peak erosion for MX-4926, clay NRAM [$(HE)_2MT$], and CNF NRAMs (PR-19 and PR-24) at three different heat flux levels with particles.

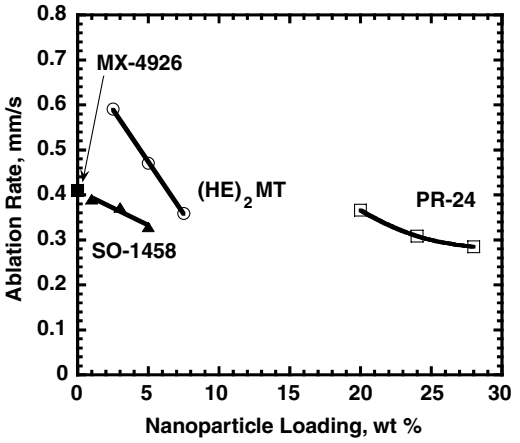

Fig. 13 Ablation rate of MX-4926 and NRAMs with different types of nanoparticles [$(HE)_2$ MT-Cloisite 30B, PR-24-PS CNF, and SO-1458 POSS] at various loading levels.

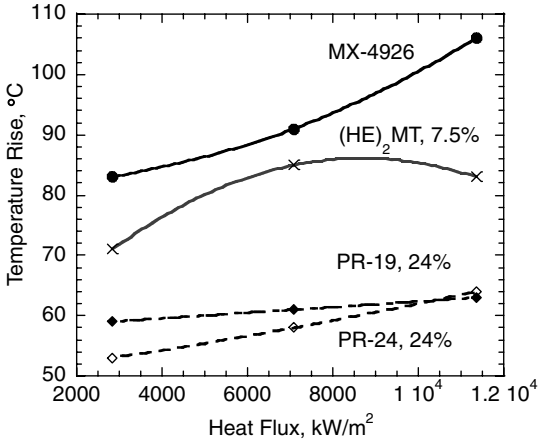

Fig. 11 Max backside heat-soaked temperature rise for MX-4926, clay NRAM [$(HE)_2MT$], and CNF NRAMs (PR-19 and PR-24) at three different heat flux levels with particles.

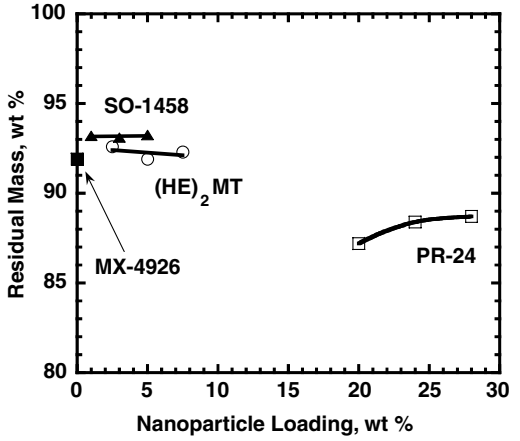

Fig. 14 Residual mass of MX-4926 and NRAMs with different types of nanoparticles [$(HE)_2$ MT-Cloisite 30B, PR-24-PS CNF, and SO-1458 POSS] at various loading levels.

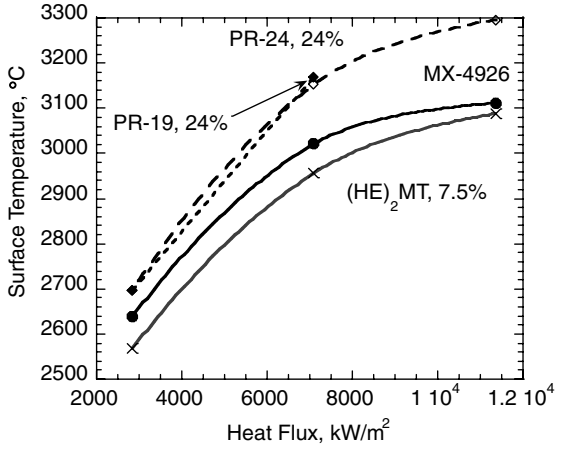

Fig. 12 Surface temperature for MX-4926, clay NRAM [$(HE)_2MT$], and CNF NRAMs (PR-19 and PR-24) at three different heat flux levels with particles.

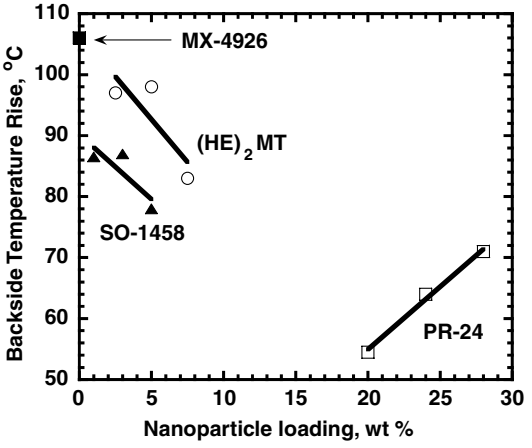

Fig. 15 Backside temperature rise of MX-4926 and NRAMs with different types of nanoparticles [$(HE)_2$ MT-Cloisite 30B, PR-24-PS CNF, and SO-1458 POSS] at various loading levels.

had essentially no effect. The amount of POSS in POSS NRAMs had a significant effect on the surface temperature of the POSS NRAMs.

From this study, the following conclusions were drawn:

1) The feasibility of using NRAMs in rocket nozzle assemblies was clearly demonstrated using SSRM subscale ablation testing.

2) MMT nanoclays, CNF, and POSS can be implemented into the existing semiproduction line at Cytec Engineered Materials to manufacture fiber-reinforced prepregs and compression molded into laminates.

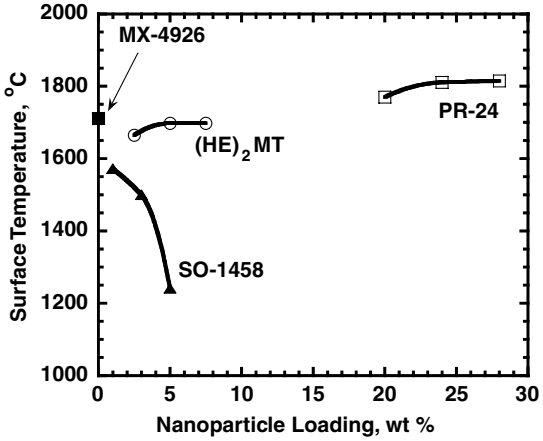

Fig. 16 Surface temperature of MX-4926 and NRAMs with different types of nanoparticles [$(HE)_2$ MT-Cloisite 30B, PR-24-PS CNF, and SO-1458 POSS] at various loading levels.

3) Higher loadings of MMT, POSS, and CNF improve erosion resistance, and 28% CNF has the lowest erosion rate in the absence of carbon fiber reinforcements.

4) Backside temperatures of all NRAMs were lower than those of baseline MX-4926, and CNF NRAM as a group had lower temperatures than the MMT NRAM and POSS NRAM groups.

5) Peak erosion of POSS NRAM is 20% lower than MX-4926 at very low loading (5% POSS).

6) Peak erosion of CNF NRAM (28% CNF) without rayon fabric is 42% lower than MX-4926.

7) Backside temperatures of CNF NRAM, MMT NRAM, and POSS NRAM are 68, 28, and 26% lower than MX4926, respectively.

B. Nanomodified Carbon–Carbon Composites

The main objective of this material program is the development of an improved carbon–carbon (C–C) composite with enhanced thermo-oxidative resistance at intermediate temperatures (370 to 650°C) [1,16–18]. The introduction of a nanophase into the C–C composite, before cure, was proposed as a means of providing improved and maintained mechanical strength by preventing oxidation of the composite. Baseline phenolic resin 134A, Hitco's precursor phenolic resin for C–C composites, and Lonza cyanate esters PT-15 and PT-30 were used as matrix resins. Hitco is a large C–C composite manufacturer involved in the development of C–C composites for many decades. Lonza's low- and medium-molecular-weight cyanate esters PT-15 and PT-30 were used as precursor resins instead of phenolic resins. Cyanate ester resins are attractive precursors for C–C composites because little or no volatiles are emitted during pyrolysis of cyanate esters. Studies by Shivakumar and others [19,20] have shown that cyanate esters can be transformed into C–C composites. Lab scale dispersion studies of these resins with selected nanoparticles such as nanoclays, CNF, and POSS at different weight percent were conducted. The morphologies of selective resin/nanoparticle systems were characterized using TEM and SEM analyses. Detailed processing and characterization of PT-30/nanoparticle, PT-15/nanoparticle, and 134A/nanoparticle systems are reported elsewhere [16–18]. A brief discussion of PT-30/nanoparticle and PT-15/nanoparticle follows.

Cloisite 30B nanoclay uniformly dispersed into both cyanate ester resins. Cloisite 30B is in an intercalated state in the PT-30, with large tactoids being observed with higher magnification (Fig. 17). Cloisite 30B dispersed more uniformly into PT-15, showing some degree of exfoliation (Fig. 18). Several different POSS materials were evaluated, and trisilanolphenyl-POSS (SO1458 POSS) was selected based on transparency, translucency, or opaqueness of the resulting

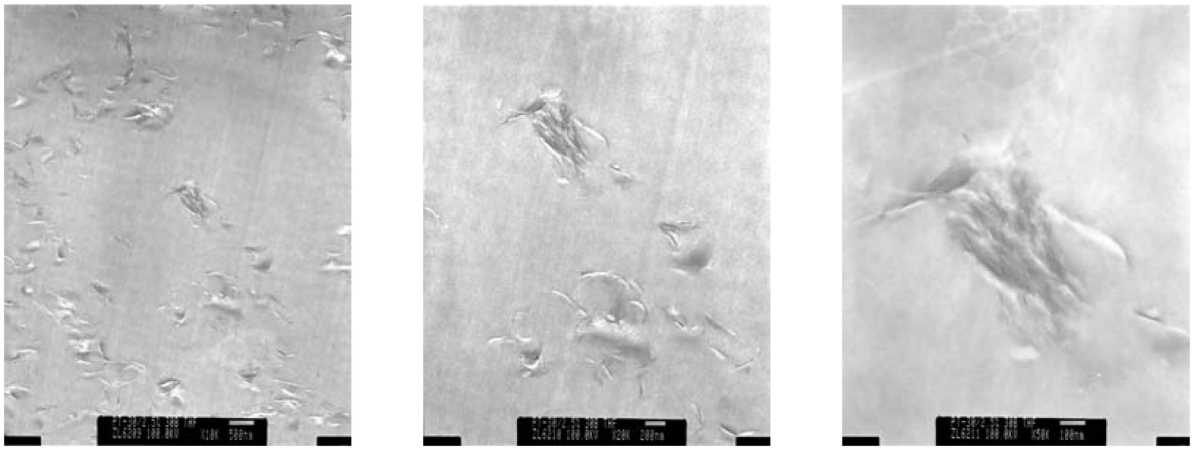

Fig. 17 Higher magnification of PT-30/Cloisite 30B (97.5/2.5) THF showing nanoclay in an intercalated state in the PT-30 cyanate ester resin, for which scale bars are 500 nm (left), 200 nm (center), and 100 nm (right).

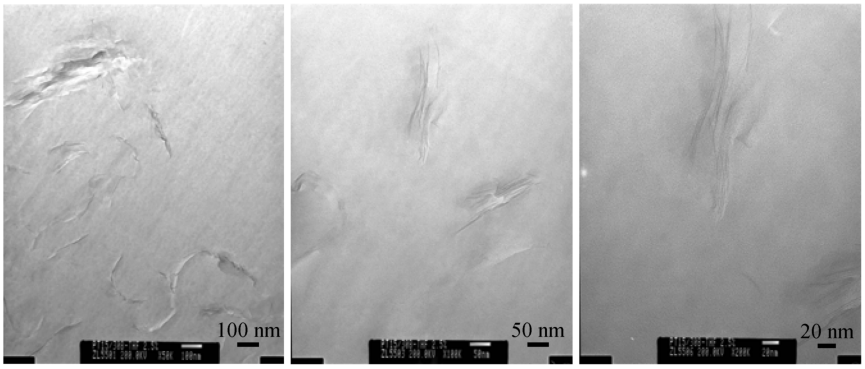

Fig. 18 Higher magnification TEM micrographs of PT-15/Cloisite 30B (97.5/2.5) THF showing Cloisite 30B clays are exfoliated in PT-15 cyanate ester.

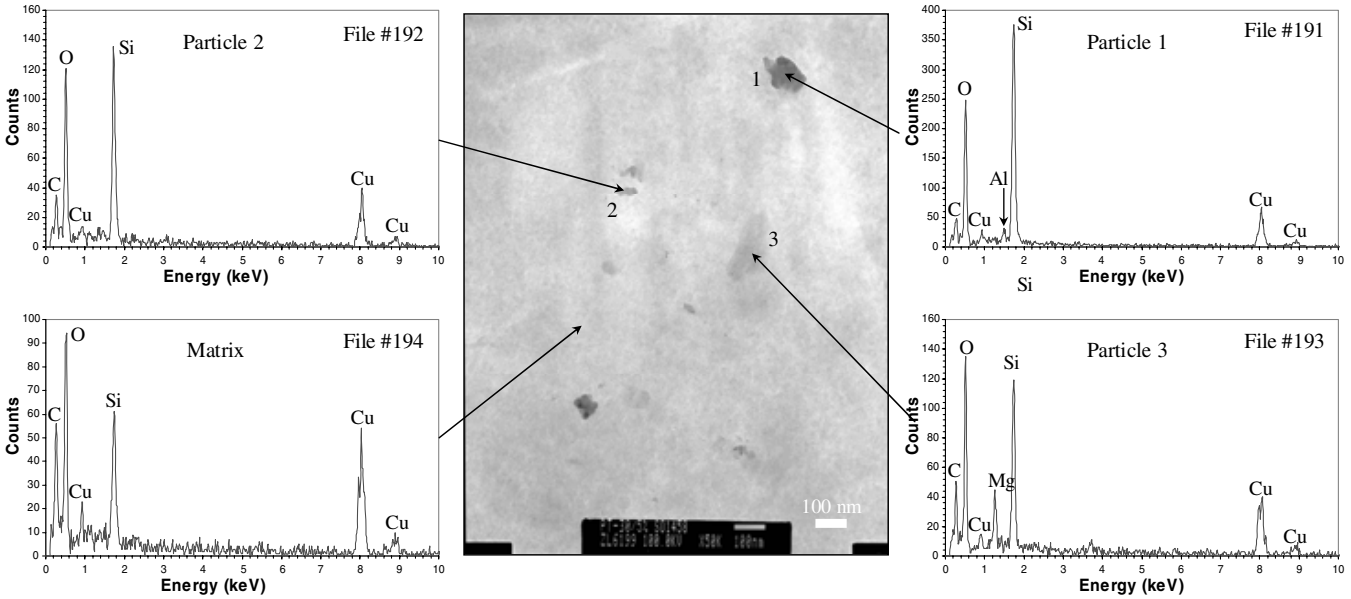

Fig. 19 TEM micrographs of PT-30/SO1458 POSS (95/5) in high magnification, showing molecular dispersion of SO1458 POSS with some POSS particles in the PT-30 cyanate ester. Significant Si is detected in the resin matrix.

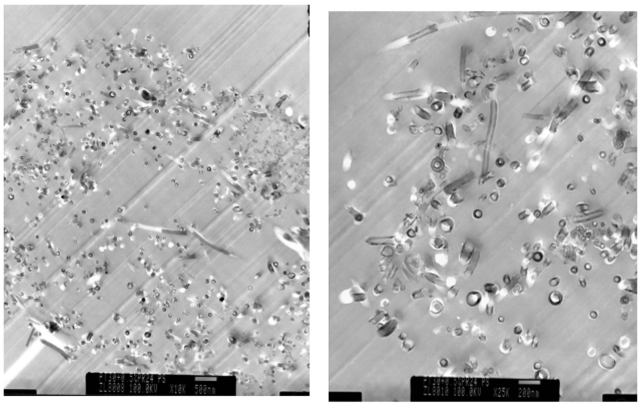

Fig. 20 TEM micrographs of PT-30/PR-24-PS (99/1) in high magnification, showing good dispersion of PR-24-PS CNF in the PT-30 cyanate ester. Scale bars are 500 nm (left) and 200 nm (right) in the TEM micrographs.

cyanate ester cured compositions. The SO1458 POSS particles, when directly blended into PT-30 resin, show very few undissolved POSS particles in the resin matrix (Fig. 19). Some molecular dispersion of SO1458 POSS occurred in the PT-30 (Fig. 19). Significant silicon is detected in the resin matrix; no phase separation can be detected. SO1458 POSS was also dispersed into PT-15 and a similar molecular dispersion of SO1458 POSS into the PT-15 was noted by TEM. Clearly, the POSS is partially dissolved in the cyanate resin matrix and partially nanodispersed, resulting in a molecular dispersion of SO1458 POSS into cyanate esters. Although POSS/PT-30 exhibited a molecular dispersion, no C–C composite data were obtained due to inadvertent air leak during pyrolysis of PT-30 into the C–C composite. CNF was also blended into PT-30 and dispersed satisfactorily (Fig. 20).

A summary of all the nanomodified carbon–carbon composite candidates and CC139 (baseline commercial carbon–carbon composite prepared with 134A phenolic resin) with their weight loss percentage, density, and ranking based on weight loss data are tabulated in Table 2. Sample designations of −1, −2, −3, and −4 are as follows: RT, 370°C, 650°C, and retained. An air leakage was detected in some of the experiments, and as a result, those specimens were overexposed to unrealistic thermo-oxidative conditions. This set of data was deleted from Table 2. The 134A/CLO/3-4B and 134A/POSS/3-4D specimens were retested for the 650°C conditions using the fourth spared panels of the 134A/CLO/3 and 134A/POSS/5 candidates marked as −4. The PT-15/POSS/5 candidate was unable to be retested for the 650°C conditions of this project. Regrettably, the behavior of molecularly dispersed POSS into PT-15 could not be assessed for improved thermo-oxidative stability due to specimens overexposed or lost.

Table 2 Summary of thermo-oxidative data and ranking[a]

P/N	Initial wt, g	TGA recorded wt, g	Weight loss, %	Sample density, g/cm^3	Rank
134A/CLO/3-4B	2.036	1.414	−30.5	1.585	6
134A/POSS/3-4D	2.055	1.573	−23.2	1.603	5
PT15/CLO/5-1	2.52	2.36	−6.5	1.63	2
PT15/CLO/5-2B	2.36	2.28	−3.4	1.643	2
PT15/CLO/5-2C	2.40	2.24	−6.8	1.643	2
PT15/CLO/5-3B	2.34	2.26	−3.5	1.684	2
PT15/CLO/5-3C	2.38	2.29	−3.8	1.684	2
PT30/PR24PS/1-3B,C	2.573	2.399	−6.8	1.684	3
PT30/CLO/5-1B,C	2.522	2.358	−5.2	1.653	1
PT30/CLO/5-2B,C	2.383	2.261	−5.1	1.656	1
PT30/CLO/5-3B,C	2.363	2.265	−3.7	1.618	1
CC139-1A	2.673	2.436	−8.9	1.627	4
CC139-2A	2.506	2.881	−9.0	1.638	4
CC139-3A	2.536	2.191	−13.6	1.630	4

[a]RT, 370°C, and 650°C specimens were designated as −1, −2, and −3, respectively.

Based on the thermo-oxidative analyses, the PT-30/CLO/5 candidate is the most thermo-oxidative-resistant material: weight losses were 5.2, 5.1, and 3.7% at room temperature (RT), 370°C, and 650°C conditions, respectively. The PT15/CLO/5 candidate is the second-best thermo-oxidative-resistant, and weight losses were 6.5, 5.1, and 3.7% at RT, 370°C, and 650°C conditions, respectively. The third-best thermo-oxidative NCCC candidate is PT-30/PR24PS/1, which had a low 6.8% weight loss at 650°C. The value is based on one sample because others like POSS/PT-30 were lost due to air leak. The standard CC139 is the fourth-best material, with a weight loss of 8.9, 9.0, and 13.6% for RT, 370°C, and 650°C conditions, respectively. The later two, 134A/CLO/3-4B and 134A/POSS/3, based on Hitco precursor phenolic resin with nanoclay and POSS, exhibited quite high weight losses of 30.5 and 23.3%, respectively, at 650°C and are based on single samples due to air leak of other samples. A comparison of weight losses (Fig. 21) identifies that cyanate ester resin-based PT-30/PR24PS/1, PT-30/CLO/5, and PT-15/CLO/5 materials have better thermo-oxidative resistance than the phenolic resin-based CC139 standard CCCs. The phenolic resin-based 134A/CLO/3 and 134A/POSS/3 specimens have worse thermo-oxidative resistance characteristics than the CC139 standard. The TEM analyses showed uniform dispersibility of nanoparticles into PT-30 and PT-15 cyanate ester resins, whereas poor dispersibility of nanoparticles occurred in 134A phenolic resin. These lend support to the observed improved performance of the nanomodified cyanate esters compared with the poor properties of the nanomodified phenolic resin.

Densities of the different NCCCs are shown in Fig. 22 and Table 2. The PT30/PR24PS/1-3B,C and PT15/CLO/5-3B,C both have the highest density (1.684 g/cm^3), followed by PT30/CLO/5-2B,C (1.656 g/cm^3) and PT30/CLO/5-1B,C (1.653 g/cm^3), then the CC139 specimens (1.627 to 1.638 g/cm^3), whereas the densities of 134A/POSS/3-4D and 134A/CLO/3-4B were 1.603 g/cm^3 and 1.585 g/cm^3, respectively. Figure 23 shows a comparison of densities versus weight loss of the different NCCCs. A trend of higher-density NCCCs exhibiting lower weight loss and lower-density NCCCs showing higher weight loss is proposed. Lower weight loss for NCCCs from cyanate ester resin is expected, owing to little or no volatiles from cured cyanate esters, as well as proposed improved thermo-oxidative stability attributable to the presence of a nanophase in the NCCC cyanate ester materials.

All four NCCCs (134A/CLO/3, 134A/POSS/3, PT30/CLO/5, and PT30/PR24PS/1) and CC139 panels were visually inspected and tap-tested to identify blisters (delamination defects) and the data were recorded. Specimens were extracted from defect-free (as much as possible) areas. All interlaminar test specimens were visually defect-free areas, whereas some tensile specimens had to be cut from the blistered areas. No blisters or delaminations were found in 134A-based panels. PT30-based panels had delaminations, blisters, and microcracks within the layer. PT30/CLO/5 panels had the greatest amount of defects. Blister diameters in PT30-based panels ranged from 2 to 5 in. in diameter. Blisters were located under the surface plies and near the midplane of the panel. All panels showed lack of or uneven densification. Macro- or microcracks or voids were apparent from 10 times and 20 times microscopy study. This finding is predominant in PT30-based panels. It was concluded that the blisters and delaminations were the result of an improper heating cycle of as-cured composite parts. Tensile specimens were selected from areas of each panel in which little or no delamination was visually detected. Tensile specimen length in the delaminated panels was increased to 12 in. to prevent splitting open the laminate at the grip ends of the coupons. Interlaminar shear strength (ILSS) specimens were selected from areas of each panel in which no delamination was visually detected and thickness was uniform.

Tension and interlaminar shear tests were conducted per ASTM D 3039-00 (tension test) and ASTM D 7904 (four-point short-beam shear test) using at least three specimens. All ILSS tests were successful and the failure modes were delaminations near the midplane, as expected. The average ILSS of CC139-4, 134A/CLO/3-4, 134A/POSS/3-4, PT30/CLO/5-4, and PT30/PR24PS/1-4 panels at room temperature were 2.8, 1.7, 1.9, 2.1, and 2.2 ksi, respectively

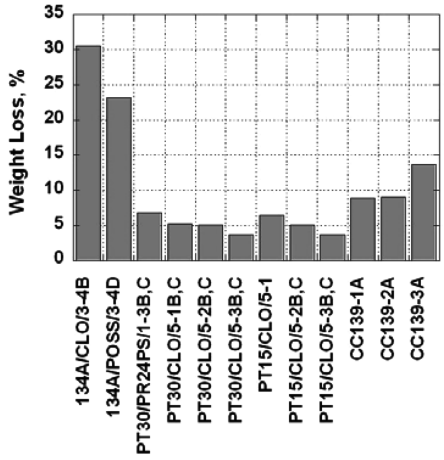

Fig. 21 Comparison of weight loss with different NCCCs.

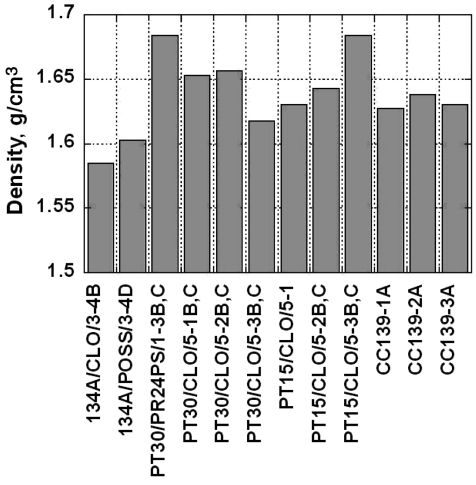

Fig. 22 Comparison of density with different NCCCs.

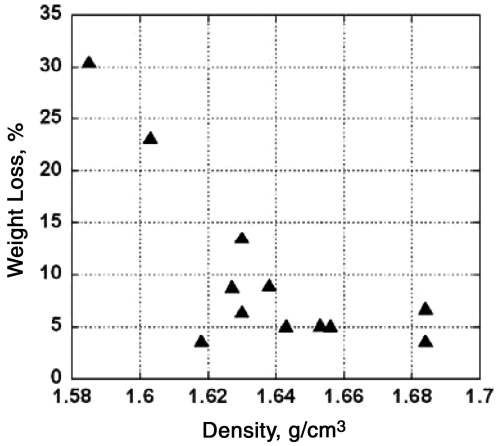

Fig. 23 Comparison of density and weight loss with different NCCCs.

[16,17]. The heat-treated (1200°F) CC139-3, PT30/CLO/5-3, PT30/PR24PS/1-3 panels lost 3, 9, and 13% of the ILSS, respectively. The room-temperature ILSS of CC139, about 2.5 ksi, agreed well with North Carolina A& T State University manufactured PT30/T300-based C–C composite panels [19,20]. Tensile modulus, tensile strength, and Poisson's ratio were measured for all five material systems. Variable tensile testing of some of the panels may be attributable to tab-slippage problems or poor interfacial bonding

Table 3 Comparison of mechanical properties of the five materials in RT and heat-aged conditions

Material	UTS, ksi	Modulus, msi	Poisson's ratio	ILSS, ksi
CC139-4	46.5	13.0	0.074	2.83
134A/CLO/3-4	53.2	17.0	0.026	1.7
134A/POSS/3-4	51.2	16.8	0.020	1.92
PT30/CLO/5-4	43.4	13.8	0.036	2.09
PTPT30PR24PS1-4	59.2	14.3	0.025	1.94
CC139-3	47.8	12.8	0.111	2.76
PT30/CLO/5-3	33.5	14.7	0.028	1.94
PT30/PR24PS/1-3	60.4	13.9	0.033	1.94

between the base material and the carbon vapor infiltration deposited carbon. The tab-slippage problem was resolved by abrading the tabbing surfaces. The room-temperature elastic moduli of CC139-4, 134A/CLO/3-4, 134A/POSS/3-4, PT30/CLO/5-4, and PT30/PR24PS/1-4 were 13.0, 17.0, 16.8, 13.8, and 14.3 msi, respectively. An increase in elastic moduli for NCCCs compared with baseline CC139 is attributed to nanophase formation. The heat-treated panels lost 3, 2, and 6% of the modulus, respectively.

The PT30/PR24PS/1-3, −4 specimens had the highest ultimate tensile strength (UTS). This material exhibited the largest maximum failure load (both RT and 650°C heat-aged specimens) and gradually fell off to 75% load until complete fracture. This finding indicated that the CNF would enhance ductility while increasing the ultimate strength of the NCCC. The nanoclay specimens were significantly weaker and also had excessive blisters. Nanoclay may adversely affect the CCC if proper heating cycling is not used in the pyrolysis of the as-cured panels. All of the PT30 materials fracture inside of the tab area, with the greatest tendency to fail at the actuator end. All PT30 materials had microcracking as well as some blistering, particularly the PT30/CLO/5-3 and −4 specimens, which had blisters near the midplane and surface plies. The strength of CC139 panels without and with heat treatment were 46.5 and 47.8 ksi; the difference is less than the one STD of the data. All nanomodified samples except PT30/CLO/5-4 exhibited a higher room-temperature strength and modulus compared with control CC139-4. Table 3 summarizes all the mechanical properties for the five materials at RT and heat-aged conditions [16,17].

The following conclusions were drawn from this study:

1) MMT clay, POSS, and CNF dispersed very well in the PT-30 and PT-15 cyanate ester resins but poorly in the 134A phenolic resin, which identified the cyanate ester nanocomposites as more desirable than the phenolic nanocomposites. Transmission electron microscopy evidence of molecular dispersion of POSS into PT-15 could not be translated into improved thermo-oxidative stability (less weight loss) because of specimen overexposure or loss.

2) The nanomodified cyanate ester CCCs (PT15/CLO/5, PT30/PR24PS/1, and PT30/CLO/5) are more thermo-oxidative-resistant than the baseline CCC (CC139). The nanomodified phenolioc CCCs (134A/CLO/3 and 134A/POSS/3) are less thermo-oxidative-resistant than the baseline CC139 material.

3) The densities of nanomodified cyanate ester CCCs (PT30/PR24PS/1, PT30/CLO/5, PT15/POSS/5, and PT15/CLO/5) were higher than that of the baseline CCC (CC139), whereas the densities of the nanomodified phenolic CCCs (134A/CLO/3 and 134A/POSS/3) were lower than those of CC139.

4) The higher-density NCCCs (based on nanomodified cyanate ester) have less weight loss than the lower-density phenolic-modified NCCC and CC139, which makes them more thermo-oxidative-resistant.

5) Blisters and delaminations of NCCCs were the result of improper heating cycle of as-cured composite parts. The use of differential scanning calorimetry (DSC) during the curing of cyanate ester resin to determine optimum cure conditions is proposed to reduce or eliminate blisters and delaminations through better cure conditions.

6) The UTS of CC139-4, 134A/CLO/3-4, 134A/POSS/3-4, PT30/CLO/5-4, and PT30/PR24PS/1-4 panels at room temperature were 46.5, 53.2, 51.2, 43.4, 59.2 ksi, respectively. Increased in the UTS of NCCCs over baseline may be attributable to nanophase formation.

7) Elastic moduli of CC139-4, 134A/CLO/3-4, 134A/POSS/3-4, PT30/CLO/5-4, and PT30/PR24PS/1-4 were 13.0, 17.0, 16.8, 13.8, and 14.3 msi, respectively. Increased elastic modulus of NCCCs over baseline may be caused by nanophase formation.

8) The average ILSS of CC139-4, 134A/CLO/3-4, 134A/POSS/3-4, PT30/CLO/5-4, and PT30/PR24PS/1-4 panels at RT were 2.8, 1.7, 1.9, 2.1, and 2.2 ksi, respectively. The heat-aged (1200°F) CC139-3, PT30/CLO/5-3, and PT30/PR24PS/1-3 panels lost 3, 9, and 13% of the ILSS, respectively.

9) The PT30/PR24PS/1-3, −4 specimens had the highest UTS. They exhibited the largest maximum failure load (for both RT and 650°C heat-aged specimens) and then gradually fell off to 75% load until complete fracture. It appears that CNF would enhance the ductility as well as increasing the ultimate strength.

10) All nanoclay NCCCs were significantly weaker and also had excessive blisters. Nanoclay may compromise the CCC if proper heating cycling is not used in the pyrolysis of the as-cured panels. Improved thermal stability surface-modified clays with alkyl imidazole surfacing agents and controlled cure (using DSC) are proposed to eliminate blisters and improve cured panel appearance and performance of nanoclay cyanate ester panels.

Table 4 Summary of DMTA analyses of epoxy nanocomposites

Material	T_g from E′, °C	T_g from E″, °C	T_g from tan δ, °C	E* at 200°C, MPa
977-3 Control	172	176	237	483
1% Cloisite 10A	183	186	245	923
2% Cloisite 10A	186	185	245	786
5% Cloisite 10A	183	185	228	572
5% Cloisite 30B	164	166	221	390
1% Aerosil R202	178	178	242	609
2% Aerosil R202	188	187	258	964
5% Aerosil R202	186	184	245	702
1% Aerosil R805	183	184	247	620
2% Aerosil R805	182	186	243	711
5% Aerosil R805	185	186	238	697
1% PR-19-PS-Ox	178	186	236	670
2% PR-19-PS-Ox	180	188	238	688
5% PR-19-PS-Ox	180	190	241	961

Table 5 Comparison of mechanical properties of six high-performance epoxy systems

Material	G_{1C}, in. · lb/in.^{2}	G_{2C}, in. · lb/in.^{2}	FWT, psi	Shear SBS, ksi	Flexural strength, ksi
977-3/2% Cloisite 10A PMC	1.10	6.02	5375	9.5	159
977-3/2% Aerosil R202 PMC	1.69	11.26	5908	10.9	141
977-3/2% Aerosil R805 PMC	1.93	12.02	5528	10.8	144
977-3/2% PR-19-PS-Ox CNF PMC	1.27	15.01	5932	12.7	142
977-3/3% Aerosil R202 PMC	1.26	11.28	5631	13.7	155
977-3/AS4-6K-HS baseline PMC	2.79	14.14	5823	11.7	150

11) All the PT-30 cyanate ester materials had microcracking as well as some blistering, particularly the nanoclay specimens, which had blisters near the midplane and surface plies.

12) Microstructure analyses of pre- and posttest NCCC specimens would gain a more fundamental understanding of material behavior. Additional research is ongoing [21].

C. Nanocomposites for Carbon-Fiber-Reinforced Polymer Matrix Composites

The major objective of this material program is to develop an improved epoxy nanocomposite carbon-fiber-reinforced PMC for missile/airframe structures with enhanced mechanical properties [1,22,23]. We proposed that a nanophase be introduced into the multifunctional epoxy resin system, before cure, to provide these features. Cytec Engineered Materials CYCOM 977-3, a damage-tolerant or toughened multifunctional epoxy carbon-fiber-reinforced polymer matrix composite, was modified with three types of nanoparticles: MMT nanoclays, CNFs, and nanosilicas at different weight loading levels (1, 2, and 5%). Analyses by TEM and SEM demonstrated that nanoparticles were dispersed into the epoxy phase. DMTA analyses were performed on selected neat cured-epoxy nanocomposites, before impregnation of the nanomodified epoxy systems onto carbon fiber. It also provided supporting evidence for the presence of nanophase in these nanocomposites by showing, in many cases, higher glass transition temperature T_g, and higher complex moduli E* than the baseline epoxy resin (Table 4). All the data are collected in three-point blending geometry with a strain amplitude of 0.05%, frequency of 1 Hz, and heating rate of 5°C/ min. The arbitrary selection of E* at 200°C was in support of T_g from dissipation factor (tan δ) data. There are some examples of increased amounts of selective nanoparticles resulting in a leveling off or reduced performance of the nanomodified epoxy resin compared with those with lesser amounts of nanoparticles. This is especially apparent when one examines DMTA data for 5% Cloisite 10A, 5% Cloisite 30B, 5% Aerosil R202, and 5% Aerosil R 805 (Table 4). Yet the use of 5% PR-19-PS-OX resulted in continuing property enhancement of the nanomodified epoxy resin (Table 4). It is unclear why the higher amount of CNF provided this increased behavior compared with the nanoclay and/or nanosilica.

Based on TEM and DMTA analyses, as well as literature data, five nanomodified compositions and the control were selected for the preparation of 20 lb of 977-3/nanoparticle resin systems to produce prepregs using AS4-6K-5HS carbon fiber. Mechanical properties such as G_{1C}, G_{2C}, FWT, SBS, and flexural strength were measured (Table 5). The G_{1C} (Fig. 24) and G_{2C} (Fig. 25) values of all the epoxy nanocomposites were below the baseline, except for 2% Aerosil R805 (G_{1C}) and 2% PR-19-PS-Ox (G_{2C}), which were higher than the baseline. No reasonable conclusion can be drawn from these data as they apply to the fiber-reinforced systems because control values were intermediate between each of the arrow bars.

The short-beam shear values of all epoxy nanocomposites were slightly lower than the baseline, with 3% Aerosil R202 and 2% PR-19-PS-Ox CNF higher than the baseline (Fig. 26). The flexural strength of all the epoxy nanocomposites was slightly lower than the baseline, with the 2% Cloisite 10A and 3% Aerosil R202 materials higher than the baseline (Fig. 27). Flatwise tension strength values of all the epoxy nanocomposites were slightly lower than the baseline, with 2% PR-19-PS-Ox and 2% Aerosil R202 samples higher than the baseline material (Fig. 28).

Higher T_g and E* observed for the neat cured 977-3 did not carry over into the carbon-fiber-reinforced system. Others [24] have also reported a similar lack of carryover of increased T_g and other properties to the fiber-reinforced composites from neat, cured, nanomodified epoxies with higher T_g. Thus, it can be concluded that nanomaterial characteristics of the epoxy resin were not applied to the resulting carbon-fiber-reinforced polymer composite. Better and more uniform interlaminar adhesion between the nanomodified

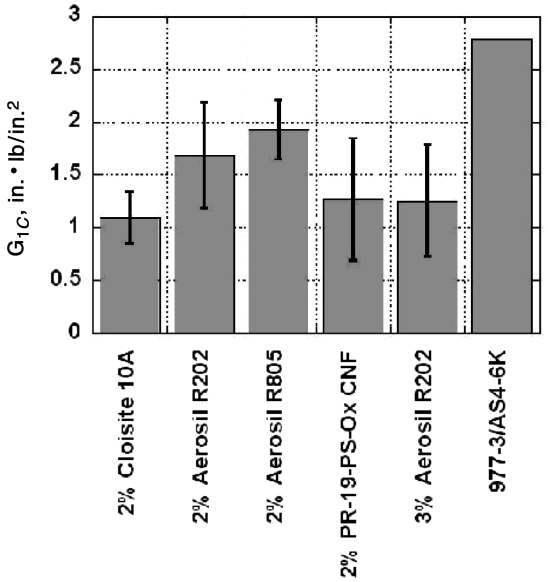

Fig. 24 Comparison of G_{1C} values of the five nanomodified epoxy carbon-fiber-reinforced PMCs with the 977-3/AS4-6K-5HS baseline composite.

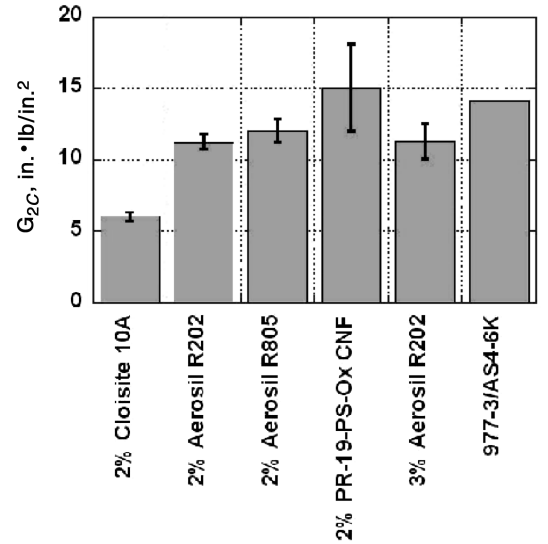

Fig. 25 Comparison of G_{2C} values of the five nanomodified epoxy carbon-fiber-reinforced PMCs with the 977-3/AS4-6K-5HS baseline composite.

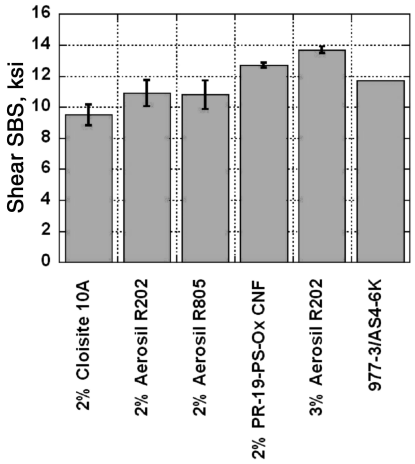

Fig. 26 Comparison of SBS values of the five nanomodified epoxy carbon-fiber-reinforced PMCs with the 977-3/AS4-6K-5HS baseline composite.

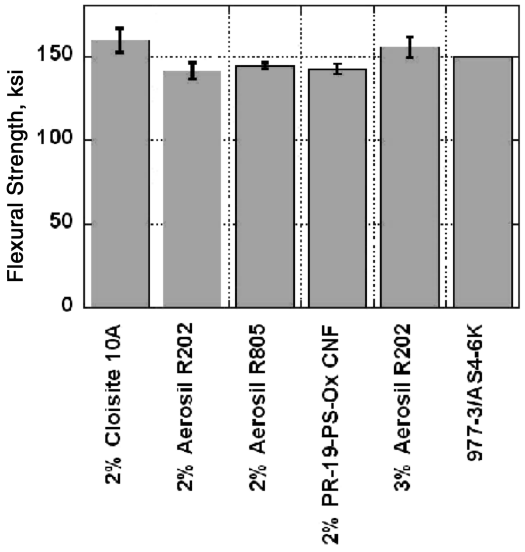

Fig. 27 Comparison of flexural strength values of the five nanomodified epoxy carbon-fiber-reinforced PMCs with the 977-3/AS4-6K-5HS baseline composite.

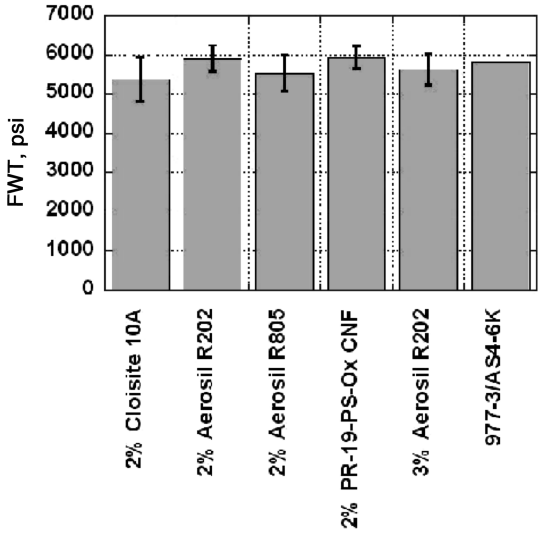

Fig. 28 Comparison of FWT values of the five nanomodified epoxy carbon-fiber-reinforced PMCs with the 977-3/AS4-6K-5HS baseline composite.

epoxy resin and carbon fiber is also proposed as providing improved properties for the final carbon-fiber-reinforced composite.

The following conclusions were drawn from this study:

1) Dynamic mechanical thermal analysis data of the neat epoxy nanosilica nanocomposites (2% Aerosil R202) show the highest T_g (258°C) and the highest E* (964 MPa).

2) Impressive values (T_g and E*) of neat nanocomposite resin with 2% Aerosil R202 did not carry over into the NCPMC.

3) MMT clay, nanosilica, and CNF dispersed very well in the 977-3 resin system, forming epoxy nanocomposites.

4) The G_{1C} values of all the epoxy nanocomposites were lower than the 977-3/AS4-K6 baseline material, with the least knockdown with the 2% Aerosil R805 nanosilica sample.

5) The G_{2C} values of all the epoxy nanocomposites were lower than the 977-3/AS4-K6 baseline material, with the 2% PT-19-PS-Ox sample higher than the baseline material

6) The FWT values of all epoxy nanocomposites were slightly lower than the baseline, and 2% PR-19-PS-Ox and 2% Aerosil R202 samples were higher than the baseline material.

7) The SBS values of all epoxy nanocomposites were slightly lower than the baseline, and 3% Aerosil R202 and 2% PR-19-PS-Ox CNF samples were higher than the baseline material.

8) The flexural strength of all epoxy nanocomposites was slightly lower than the baseline, and the values for 2% Cloisite 10A and 3% Aerosil R202 samples were higher than the baseline.

V. Conclusions

Polymer nanocomposites were developed to enhance material properties for high-temperature applications. The following conclusions are presented:

1) The feasibility of using polymer nanocomposites for high-temperature applications is clearly demonstrated for rocket nozzle ablative materials, carbon–carbon composites, and damage-tolerant high-performance epoxy carbon-fiber-reinforced composite systems.

2) MMT organoclay, nanosilica, CNF, and POSS can be easily incorporated into various polymers using high-shear processing and appropriate manufacturing techniques to form polymer nanocomposites.

3) The desired level and uniformity of nanoparticle dispersion in the polymer matrix as intercalated or well-dispersed achieves the desired properties' enhancement in the resulting cured polymer nanocomposite resin matrix.

4) TEM analyses techniques are demonstrated to be effective and efficient screening "tools" to determine nanodispersion in the polymer matrix. Many poorly dispersed samples consisting of various POSS materials and other nanoparticles were discarded due to nonuniformity in dispersion. SEM was effective in characterizing morphology and surface of ablative NRMAs.

Acknowledgments

The authors would like to thank Charles Y-C Lee of the U.S. Air Force Office of Scientific Research (AFOSR) for sponsoring several of our research activities through the AFOSR Small Business Technology Transfer Program. Support from Shawn Phillips of the U.S. Air Force Research Laboratory (AFRL) at Edwards Air Force Base is also appreciated. Others who provided assistance include Abdel Abusafieh, Flake Campbell Jr., Sajal Das, Alan Hedgepeth, Doug Hunter, Max Lake, Joseph Lichtenhan, Zhiping Luo, Holly Stretz, and Jon Weispfenning. The authors also would like to express their appreciation to numerous colleagues who have contributed to our nanomaterials research.

References

[1] Koo, J. H., *Polymer Nanocomposites: Processing, Characterization, and Applications*, McGraw–Hill, New York, 2006.

[2] Pinnavaia, T. J., and Beall, G. W. (eds.), *Polymer-Clay Nanocomposites*, Wiley, New York, 2000.

[3] Krishnamoorti, R., and Vaia, R. A. (eds.), *Polymer Nanocomposites:*

Synthesis, Characterization, and Modeling, ACS Symposium Series 804, American Chemical Society, Washington, DC, 2001.

[4] Tibbetts, G. G., "Why are Carbon Filaments Tubular?," *Journal of Crystal Growth*, Vol. 66, 1984, 632–638.

[5] Lake, M. L., and Ting, J-M., "Vapor Grown Carbon Fiber Composites," *Carbon Materials for Advanced Technologies*, edited by T. D. Burchell, Pergamon, Oxford, 1999.

[6] Tibbetts, G. G., Lake, M. L., Karla, K. L., and Rice, B. P., "A Review of the Fabrication and Properties of Vapor-Grown Carbon Nanofiber/Polymer Composites," *Composites Science and Technology*, Vol. 67, 2007, pp. 1709–1718.

[7] Maruyama, B., and Alam, K., "Carbon Nanotubes and Nanofibers in Composite Materials," *SAMPE Journal*, Vol. 38, No. 3, 2002, p. 59.

[8] Koo, J. H., Stretz, H., Bray, A., Wootan, W., Mulich, S., Powell, C., Weispfenning, J., and Grupa, T., "Phenolic-Clay Nanocomposite Ablatives for Rocket Propulsion Systems," *Proceedings of the International SAMPE 2002 Symposium and Exhibition*, Society for the Advancement of Material and Process Engineering, Covina, CA, 2002, p. 1085.

[9] Koo, J. H., Stretz, H., Bray, A., Weispfenning, J., Luo, Z. P., and Wootan, W., "Nanocomposite Rocket Ablative Materials: Processing, Characterization, and Performance," *Proceedings of the International SAMPE 2003 Symposium and Exhibition*, Society for the Advancement of Material and Process Engineering, Covina, CA, 2003, p. 1156.

[10] Koo, J. H., Chow, W. K., Stretz, H., Cheng, A. C-K., Bray, A., and Weispfenning, J., "Flammability Properties of Polymer Nanostructured Materials," *Proceedings of the International SAMPE 2003 Symposium and Exhibition*, Society for the Advancement of Material and Process Engineering, Covina, CA, 2003, p. 954.

[11] Koo, J. H., Stretz, H., Weispfenning, J., Luo, Z., and Wootan, W., "Nanocomposite Rocket Ablative Materials: Subscale Ablation Test," *Proceedings of the International SAMPE 2004 Symposium* [CD-ROM], Society for the Advancement of Material and Process Engineering, Covina, CA, 2004.

[12] Koo, J. H., Stretz, H., Weispfenning, J., Luo, Z., and Wootan, W., "Nanocomposite Rocket Ablative Materials: Processing, Microstructures, and Performance," AIAA Paper 2004-1996, Apr. 2004.

[13] Koo, J. H., Kneer, M., and Schneider, M., "A Cost-Effective Approach to Evaluate High-Temperature Ablatives for Military Applications," *Naval Engineers Journal*, Vol. 104, 1992, pp. 166–177.

[14] Miller, M. J., Koo, J. H., and Lin, S., "Evaluation of Different Categories of Composites Ablative for Thermal Protection," AIAA Paper 93-0839, Jan. 1993.

[15] Patton, R. D., Pittman, C. U., Wang, L., Hill, J. R., and Day, A., "Ablation, Mechanical and Thermal Conductivity Properties of Vapor Growth Carbon Fiber/Phenolic Matrix Composites," *Composites, Part A: Applied Science and Manufacturing*, Vol. 33, 2002, pp. 243–251.

[16] Koo, J. H., Pittman, C. U., Jr., Liang, K., Cho, H., Pilato, L., Luo, Z. P., Pruett, G., and Winzek, P., "Nanomodified Carbon/Carbon Composites for Intermediate Temperature: Processing and Characterization," *Proceedings of the 35th International SAMPE Technical Conference* [CD-ROM], Society for the Advancement of Material and Process Engineering, Covina, CA, 2003.

[17] Koo, J. H., Pilato, L., Winzek, P., Shivakumar, K., Pittman, C. U., Jr., and Luo, Z. P., "Thermo-Oxidative Studies and Mechanical Properties of Nanomodified Carbon/Carbon Composites," *Proceedings of the International SAMPE 2004 Symposium and Exhibition* [CD-ROM], Society for the Advancement of Material and Process Engineering, Covina, CA, 2004.

[18] Liang, K., Li, G., Toghiani, H., Koo, J. H., and Pittman, C. U., Jr., "Cyanate Ester/Polyhedral Oligomeric Silsesquioxane (POSS) Nanocomposites: Synthesis and Characterization," *Chemistry of Materials*, Vol. 18, 2006, pp. 301–312.

[19] Shivakumar, K., Abali, F., and Sadler, R., "Development of Cyanate Ester Based Carbon/Carbon Composites," *Proceedings of the International SAMPE 2000 Symposium and Exhibition*, Society for the Advancement of Material and Process Engineering, Covina, CA, May 2000, pp. 1005–1015.

[20] Abali, F., Shivakumar, K., Hamidi, N., and Sadler, R., "An RTM Densification Method of Manufacturing Carbon–Carbon Composites Using Primaset PT-30 Resin," *Carbon*, Vol. 41, No. 5, 2003, pp. 893–901.

[21] Koo, J. H., Lao, S., Jor, A., Pilato, L. A., J. Lee, J., Wissler, G., and Luo, Z. P., "Thermo-Oxidative Studies of Nanomodified Carbon/Carbon Composites: Processing and Microstructural Characterization," *Proceedings International SAMPE 2007 Symposium and Exhibition* [CD-ROM], Society for the Advancement of Material and Process Engineering, Covina, CA, 2007.

[22] Koo, J. H., Pilato, L., Wissler, G., Lee, A., and Luo, Z., "Nanocomposites for Carbon Fiber-Reinforced Polymer Matrix Composites," AIAA Paper 2005-1928, Apr. 2005.

[23] Koo, J. H., Pilato, L., Wissler, G., Abusafieh, A., and Weispfenning, J., "Epoxy Nanocomposites for Carbon Fiber-Reinforced Composites," *Proceedings of the International SAMPE 2005 Symposium and Exhibition* [CD-ROM], Society for the Advancement of Material and Process Engineering, Covina, CA, 2005.

[24] Rice, B. P., Gibson, T., and Lafdi, K., "Development of Multifunctional Advanced Composites Using a VGNF Enhanced Matrix," *Proceedings of the International SAMPE 2004 Symposium and Exhibition* [CD-ROM], Society for the Advancement of Material and Process Engineering, Covina, CA, 2004.

K. Wurster
Associate Editor